DEPARTMENT OF PHYSICS
UNIVERSITY OF JYVÄSKYLÄ
RESEARCH REPORT No. 3/2017

THEORETICAL STUDY OF SUPERNOVA NEUTRINO AND ANTINEUTRINO SCATTERING OFF THE STABLE CADMIUM AND LEAD ISOTOPES

BY
Wafa Almosly

Academic Dissertation
for the Degree of
Doctor of Philosophy

To be presented, by permission of the
Faculty of Mathematics and Natural Sciences
of the University of Jyväskylä,
for public examination in Auditorium FYS1 of the
University of Jyväskylä on April 7, 2017
at 12 o'clock noon

Jyväskylä, Finland

Preface

The work presented in this thesis has been carried out at the department of physics of the university of Jyväskylä during the years 2013-2016. This work was supported by the Academy of Finland under the Finnish Center of Excellence Program 2012-2017 (Nuclear and Accelerator Based Program at JYFL).

I am especially grateful to my supervisor Prof. Jouni Suhonen for giving me the opportunity to work on such a fascinating project. Thanks for the excellent guidance and meticulous suggestions. I am very thankful for Dr. Emanuel Ydrefors for the excellent collaboration and great advice regarding the computer programs. My thanks also goes to Prof. Gabriel Martínez-Pinedo and Prof. Nils Paar for reviewing my manuscript.

I would like to thank all friends and colleagues. Special thanks for the whole staff at the physics department for the nice working atmosphere.

Above all, I am deeply indebted to my parents, Safa and Mohamed Safouh, for their love and unfailing encouragement. Thank you both for supporting me to raise my own potential. Many thanks to my brother, Ibrahem, for all the love and encouragement.

Last but far from least, I wish to express my deep gratitude to Nael, my husband, for his continued encouragement. This journey would not have been possible without his support and love. Many thanks to my two lovely children, Rand and Nour Eddin, who make my life very colorful. I would like to take this opportunity to wish them a happy and successful future.

Abstract

In this thesis work, an extensive study of neutrino- and antineutrino-nucleus interactions is performed. The work is focused on supernova-neutrino scattering off the stable cadmium and lead isotopes. The studied nuclei are of interest for the investigations of neutrino-properties and for neutrino-detection experiments.

The adopted nuclear-structure models are based on the quasiparticle random-phase approximation (QRPA) and the microscopic quasiparticle-phonon model (MQPM) and the cross-sections calculations are based on the Donnelly-Walecka formalism. The computed cross sections are folded with a two-parameter Fermi-Dirac distribution to obtain realistic estimates of the nuclear responses to supernova neutrinos.

This thesis consists of two parts, an overview part and publications part. The overview part summarized the main aspect of the performed studies of the five publications presented in the second part.

Author's address Wafa Almosly
Department of Physics
University of Jyväskylä
Finland

Supervisor Professor Jouni Suhonen
Department of Physics
University of Jyväskylä
Finland

Reviewers Professor Gabriel Martínez-Pinedo
Institut für Kernphysik
Technische Universität Darmstadt
Germany

Professor Nils Paar
Department of Physics
University of Zagreb
Croatia

Opponent Professor Natalie Jachowicz
Ghent University
Belgium

Publications

I. W. Almosly, E. Ydrefors and J. Suhonen, *Neutral- and charged-current supernova-neutrino scattering off* ^{116}Cd, J. Phys. G: Nucl. Part. Phys. **40** (2013) 095201.

II. W. Almosly, B. G. Carlsson, J. Dobaczewski, J. Suhonen, J. Toivanen, P. Vesely and E. Ydrefors, *Charged-current neutrino and antineutrino scattering off* ^{116}Cd *described by Skyrme forces*, Phys. Rev. C. **89** (2014) 024308.

III. W. Almosly, E. Ydrefors and J. Suhonen, *Neutrino scattering off the stable cadmium isotopes: neutral-current processes*, J. Phys. G: Nucl. Part. Phys. **42** (2015) 025106.

IV. W. Almosly, E. Ydrefors and J. Suhonen, *Neutrino scattering off the stable cadmium isotopes: II. Charged-current processes*, J. Phys. G: Nucl. Part. Phys. **42** (2015) 095106.

V. W. Almosly, B. G. Carlsson, J. Suhonen, J. Toivanen and E. Ydrefors, *Theoretical estimates of supernova-neutrino cross sections for the stable even-even lead isotopes: Charged-current reactions*, Phys. Rev. C. **94** (2016) 044614.

The author of the present thesis has performed all the numerical calculations and written the first draft of the listed publications.

Contents

1. Introduction

Neutrino-nucleus interactions are of great interest in modern physics as a tool to explore several interesting phenomena such as supernova explosions and supernova nucleosynthesis. In addition, the neutrino interactions provide a wealth of information for the theory of weak interactions as well as on neutrino properties. Studies of neutrino properties are in general of high importance for completing our picture of this fundamental particle. We know nowadays that the neutrino undergoes flavor transformations and it is not a massless particle. However, the absolute value of the neutrino mass, the neutrino-mass hierarchy, and the nature of neutrino (a Dirac or a Majorana particle) is still under vigorous investigation.

Neutrinos that emerge after the core collapse of heavy stars give information about the very early stages of the collapse. The neutrino signal can be detected by Earth-bound neutrino and antineutrino telescopes using charged-current and/or neutral-current neutrino scatterings off nuclei. Several neutrino-detector facilities are being established and planned around the world for the detection of the core-collapse associated neutrinos [1]. Current and future detectors use carbon, oxygen, argon and lead. Heavy nuclei such as lead were proposed to be used in order to increase the neutrino cross section [2]. Neutrino-lead detectors are in use at the HALO experiment (Helium And Lead Observatory) [3]. HALO is a supernova-neutrino detector running at SNOLAB, Canada [4]. Theoretical estimates of neutrino-nucleus cross sections will be an important key in the interpretations of this and other measurements.

Moreover, a detailed knowledge about the nuclear responses to supernova neutrinos is essential for the study of supernova mechanisms and the nucleosynthesis of heavy elements [5, 6]. The responses serve also as probes of neutrino properties [7]. Neutral-current neutrino-nucleus interaction for example is flavor independent and can be used for the detection of muon and tau neutrinos. The cross sections of the charged-current reactions can be used in the studies of neutrinoless double-beta decay [8]. This process ($0\nu\beta\beta$) can take place if the neutrino is a Majorana particle. Therefore, if

the neutrinoless double beta decay is observed it will give an answer to the question of the nature of neutrino and also measure the neutrino mass [9, 10]. One presently running experiment for such studies is the COBRA (Cadmium Zinc Telluride 0-Neutrino Double-Beta Research Apparatus) running in Gran Sasso National Laboratory in Italy [11]. Cadmium nuclei are also interesting candidates for several theoretical studies of double beta decay [12, 13, 14].

Supernova neutrino-nucleus cross sections of neutral-current and charged-current scattering off different target nucleus have been studied using a variety of theoretical approaches. The reaction on ^{12}C and ^{16}O, for example, has been studied using random-phase approximation (RPA) [15], Continuum RPA [16, 17, 18, 19], relativistic quasiparticle random-phase approximation (RQRPA) [20, 21], and projected QRPA [22]. Calculations based on shell model has been done for ^{16}O [23] and for ^{56}Fe and ^{56}Ni [24]. The thermal QRPA was adopted in [25] for ^{56}Fe and ^{82}Ge. The QRPA is the model of choice for neutrino scattering off even Mo isotopes [26], ^{136}Xe [27] and ^{12}C, ^{56}Fe and ^{56}Ni [28]. The relativistic nuclear energy density fucctional is used for the charged-current reaction with ^{12}C, ^{16}O, ^{56}Fe and ^{208}Pb [29].

The purpose of the present work is to study the neutral-current and charged-current (anti)neutrino-nucleus scattering off the stable cadmium and lead isotopes. The cross section were computed for neutrino energies relevant for supernova neutrinos. To this aim, the required wave functions for the initial and all possible final nuclear states are computed first by using the quasiparticle random-phase approximation for the even-mass target nuclei and the microscopic quasiparticle-phonon model for the odd-mass cadmium nuclei. The double-differential cross section are subsequently computed. The nuclear responses are then estimated by folding the cross sections with realistic energy profiles for the incoming (anti)neutrinos.

2. Theoretical Framework

This chapter introduces briefly the main ingredients of the adopted nuclear-structure framework and neutrino-nucleus interaction formalism.

The quasiparticle random-phase approximation (QRPA) in its charge-conserving mode and charge-changing mode is adopted to construct the initial and final nuclear states that are relevant for (anti)neutrino scattering off the studied even-mass target nuclei, see [30] for a comprehensive discussion of the QRPA model. The microscopic quasiparticle-phonon model (MQPM) [31] is used in the case of odd-mass target nuclei.

The cross-section calculations are based on the Donnelly-Walecka method for treatment of semi-leptonic processes in nuclei [32] . The formalism is reviewed in great detail in [33] for the neutral-current reactions and in [34] for the charged-current reactions.

2.1 Nuclear Structure

2.1.1 Nuclear mean field

An exact description of a nuclear system with A strongly interacting nucleons is a challenging problem. One needs an elegant approximation to handle such a many-body system. The mean-field approximation is usually used as a starting point for solving this problem. Each nucleon in this approximation is considered as independent particle moving in an average field created by the other remaining nucleons in the nucleus. The nuclear Hamiltonian can then written as

$$H = H_{\mathrm{MF}} + V_{\mathrm{RES}} \tag{2.1}$$

where H_{MF} is the mean-field Hamiltonian and V_{RES} is the residual interaction.

The mean field potential can be generated either by a self-consistent Hartree-Fock procedure or by the use of a realistic phenomenological potential like Woods-Saxon potential.

In open-shell nuclei, i.e. nuclei with several nucleons outside closed major shells, the particle-hole methods become inapplicable. It is found appropriate to introduce the concept of a quasiparticle which mixes the particle and hole degrees of freedom. The simple quasiparticle shell model consists of a quasiparticle vacuum and non-interacting quasiparticles. Moreover, the pairing interaction in nuclei is also important for the description of open-shell nuclei. There is much experimental evidence of the pairing phenomenon in nuclei. For example, the fact that the ground state of every known even-even nucleus is a state of zero angular momentum (0^+ state). The odd-even mass difference serves as another evidence. The pairing phenomenon is also present in superconductors. The BCS theory [35] has been adopted for the theoretical treatment of superconductivity. It was proposed to be used in nuclear systems by Bohr, Mottelson and Pines [36].

The BCS quasiparticle creation and annihilation operators can be defined as liner combinations of the mean-field particle creation and annihilation operators via the standard Bogoliubov-Valantin transformation

$$a^\dagger_\alpha = u_a c^\dagger_\alpha + \upsilon_a \tilde{c}_\alpha, \tag{2.2}$$

$$\tilde{a}_\alpha = u_a \tilde{c}_\alpha - \upsilon_a c^\dagger_\alpha, \tag{2.3}$$

where υ_a and u_a are occupation and unoccupation amplitudes, respectively, that are obtained by minimizing the energy of the BCS ground state [30]

$$|\mathrm{BCS}\rangle = \prod_{\alpha>0}(u_a - \upsilon_a c^\dagger_\alpha \tilde{c}^\dagger_\alpha)|\mathrm{HF}\rangle. \tag{2.4}$$

The nuclear Hamiltonian in this representation can be written as

$$H = H_{11} + H_{02} + H_{20} + H_{13} + H_{31} + H_{40} + H_{04}, \tag{2.5}$$

where the numbers in each term denote the number of quasiparticle creation and annihilation operators, respectively. The terms H_{02} and H_{20} vanish as a result of the minimization process. The first term then describes the quasiparticle mean field and the rest of the terms constitute the residual interaction.

In the BCS calculations the interaction matrix elements for protons and neutrons are scaled separately by a constant so that the lowest quasiparticle energies can be set equal to the experimental pairing gaps. This is the standard way of fixing the absolute scale of the quasiparticle energy spectrum.

2.1.2 Quasiparticle random-phase approximation (QRPA)

The QRPA method [30] handles the configuration mixing between two-quasiparticle states caused by the terms H_{40} and H_{04} of the residual interaction

of the Hamiltonian (2.5). The charge-conserving QRPA can be used for the description of the states in a spherical even-even nucleus. The charge-changing QRPA or the so-called proton-neutron QRPA (pnQRPA) describes the states of an odd-odd nucleus with respect to an even-even QRPA ground state. The excited states in the QRPA theory are formed by coupling two-quasiparticle operators to good angular momentum

$$|\omega\rangle = |J_\omega \pi_\omega M_\omega\rangle = Q^\dagger_\omega |\mathrm{QRPA}\rangle \tag{2.6}$$

where $|\mathrm{QRPA}\rangle$ denotes the QRPA ground state that acts as a vacuum and the Q_ω is the QRPA excitation operator

$$Q^\dagger_\omega = \sum_{a\leq b} N_{ab}(J_\omega) \left[X^\omega_{ab} [a^\dagger_a a^\dagger_b]_{J_\omega M_\omega} + Y^\omega_{ab} [\tilde{a}_a \tilde{a}_b]_{J_\omega M_\omega} \right], \tag{2.7}$$

where the indices a and b run over all two-proton and two-neutron configurations within the chosen valence space, so that non of them is counted twice. The X^ω_{ab} is called the forward-going amplitude and Y^ω_{ab} is backward-going amplitude. The $N_{ab}(J_\omega)$ is a normalizing factor. Similarly, the proton-neutron QRPA excitation operator can be written in the form

$$Q^\dagger_\omega = \sum_{pn} \left[X^\omega_{pn} [a^\dagger_p a^\dagger_n]_{J_\omega M_\omega} + Y^\omega_{pn} [\tilde{a}_p \tilde{a}_n]_{J_\omega M_\omega} \right], \tag{2.8}$$

where the indices run over all possible proton-neutron configurations in the adopted valence space.

The amplitudes X^ω_{ab} and Y^ω_{ab} can be solved from the matrix equation

$$\begin{pmatrix} A & B \\ -B^* & -A^* \end{pmatrix} \begin{pmatrix} X^\omega \\ Y^\omega \end{pmatrix} = E_\omega \begin{pmatrix} X^\omega \\ Y^\omega \end{pmatrix} , \tag{2.9}$$

where E_ω is the excitation energy of the state $|\omega\rangle$. The submatrix A is a Hermitian matrix and known as Tamm-Dancoff matrix (QTDA matrix) in the case of QRPA and pnQTDA matrix in the case of pnQRPA. The submatrix B is symmetric and called the correlation matrix since it contains the ground-state correlations.

The interaction matrix elements are scaled in practice by two coefficients: g_{pp} and g_{ph} [37]. These parameters are usually adjusted for each multipole separately to fit available empirical data such as the energy of the Gamow-Teller giant resonance excitation, experimental energies of nuclear levels, and $\log ft$ values of β^+ or β^- transitions.

2.1.3 Microscopic quasiparticle-phonon model (MQPM)

The MQPM model [31] is used in our works for the nuclear structure of odd-mass target nuclei and their adjacent isobars. The MQPM diagonalizes the parts H_{31} and H_{13} of the residual Hamiltonian (2.5) in a model space consisting of one-quasiparticle and three-quasiparticle basis states. The three-quasiparticle states in this model are constructed by coupling one-quasiparticle states of the BCS and QRPA phonons of an even-even reference nucleus. The MQPM excitation operator then reads

$$\Gamma_k^\dagger(jm) = \sum_n X_n^k a_{njm}^\dagger + \sum_{a\omega} X_{a\omega}^k [a_a^\dagger Q_\omega^\dagger]_{jm}. \tag{2.10}$$

This operator creates a state with angular momentum j and z-projection m. The index k enumerates states with the same j^π. The expansion amplitudes X_n^k and $X_{a\omega}^k$ are obtained by solving the MQPM equations of motion that lead to a generalized real eigenvalue problem

$$\begin{pmatrix} A & B \\ -B^{\mathrm{T}} & A' \end{pmatrix} \begin{pmatrix} X_n^k \\ X_{a\omega}^k \end{pmatrix} = E_k \begin{pmatrix} 1 & 0 \\ 0 & N \end{pmatrix} \begin{pmatrix} X_n^k \\ X_{a\omega}^k \end{pmatrix} , \tag{2.11}$$

where N is the overlap matrix containing overlaps between two three-quasiparticle states. The matrices A, A' and B represent the interaction between two one-quasiparticle states, between two two-quasiparticle states, and between a one-quasiparticle state and a two-quasiparticle state, respectively. The explicit form of these matrices and the procedure for solving the eigenvalue problem in an overcomplete one-phonon plus three-phonon basis is described in detail in [31].

2.1.4 Two-body interactions used in the calculations

The calculations in my publications I, III, IV were performed by adopting the Bonn one-boson-exchange potential [38] as the two-body nucleon-nucleon interaction. The pairing part and the multipole parts of this interaction were scaled by the coefficients derived from phenomenology as described in sections 2.1.1 and 2.1.2. Since the nuclear mean field is generated by the Woods-Saxon potential and not by the Bonn potential, the calculations are not self-consistent.

The nuclear wave functions which are required in our studies of the charged-current neutrino and antineutrino scattering off ^{116}Cd and lead isotopes (my publications II and V) were built using a Skyrme-based pnQRPA. The pnQRPA calculations were done by exploiting the full diagonalization method implemented in the code HOSPHE [39]. The quasiparticle ground

state is obtained using the Hartree-Fock-Bogolubov (HFB) approach. The Skyrme two-body interactions are employed to produce an effective short-range interaction. The same Skyrme interaction is also used as the proton-neutron particle-hole residual interaction and hence the calculations are self-consistent. The used Skyrme interactions are density dependent two-body interactions with phenomenological fitting of the force parameters.

In the works II and V a gaussian-type pairing interaction in a separable form [40] is adopted. The pairing interaction is parametrized with two different strengths G_0 and G_1 for the $T = 0$ (isoscalar) and $T = 1$ (isovector) channels [41], respectively. The $T = 0$ pairing channel is not active in the HFB calculation. This part of the pairing can lead to pn-pairing condensates in $Z = N$ nuclei if the interaction strength is taken to be strong enough. Therefore the value of G_0 is not determined at the HFB level and thus it should be fitted separately. However, it is found appropriate, using the experimental data on odd-odd nuclei, to choose $G_0 = G_1$.

2.2 Neutrino-nucleus scattering

Neutrino-nucleus interactions are classified into two processes: the neutral-current (NC) and charged-current (CC) ones, depending on the exchanged particle (Z or W boson). In the first case, both the scattered (anti)neutrino and the target nucleus preserve their nature

$$\nu_l + (A, Z) \rightarrow (A, Z)^* + \nu_l', \tag{2.12}$$
$$\bar{\nu}_l + (A, Z) \rightarrow (A, Z)^* + \bar{\nu}_l', \tag{2.13}$$

whereas the CC reaction leads to a different nucleus and a charged lepton is emitted

$$\nu_l + (A, Z) \rightarrow (A, Z + 1) + l^-, \tag{2.14}$$
$$\bar{\nu}_l + (A, Z) \rightarrow (A, Z - 1) + l^+, \tag{2.15}$$

where l stands for either an electron (e), muon (μ) or tau (τ) lepton. In the NC reaction the final state is either the same state (coherent scattering) or an excited state (incoherent scattering) of the target nucleus. Only incoherent scattering is considered in this work. However, in the CC reactions the final state is either the ground state or an excited state of the final nucleus. Moreover, only electron or positron are emitted in the case of CC supernova-neutrino scattering due to the moderate energy of the impinging (anti)neutrino.

Supernova neutrinos have low energies typically $E_\nu \lesssim 100\,\mathrm{MeV}$. The transferred four-momentum in this low energy is small compared to the mass of the exchanged boson. The matrix element of the effective Hamiltonian can then be written in the form

$$\langle f|H_{\mathrm{eff}}|i\rangle = \frac{G}{\sqrt{2}}\int d^3\mathbf{r} l_\mu \mathrm{e}^{-\mathrm{i}\mathbf{q}\cdot\mathbf{r}}\langle f|\mathcal{J}^\mu(\mathbf{r})|i\rangle, \tag{2.16}$$

where $\mathcal{J}^\mu(\mathbf{r})$ denotes the hadron current and l_μ is the lepton matrix element, $l_\mu = \mathrm{e}^{\mathrm{i}\mathbf{q}\cdot\mathbf{r}}\langle \mathrm{f}|\mathrm{j}_\mu(\mathrm{r})|\mathrm{i}\rangle$. The constant G is the Fermi constant $G = G_{\mathrm{F}} = 1.1644 \times 10^{-5}$ GeV in the case of NC reaction and $G = G_{\mathrm{F}}\cos\theta_{\mathrm{C}}$ in the case of CC reaction, where $\theta_{\mathrm{C}} = 13^\circ$ denotes the Cabibbo angle.

We assume that the final and initial states have a well-defined angular momenta and parities. Consequently, the double-differential cross section corresponding to the NC process is given by

$$\Big[\frac{\mathrm{d}^2\sigma_{\mathrm{i}\to\mathrm{f}}}{\mathrm{d}\Omega\mathrm{d}\mathrm{E}_{\mathrm{exc}}}\Big]_{\nu_{\mathrm{e}}/\bar{\nu}_{\mathrm{e}}} = \frac{G_{\mathrm{F}}^2|\mathbf{k}'|E_{\mathbf{k}'}}{\pi(2J_i+1)} \times \Big(\sum_{J\geqslant 0}\sigma_{\mathrm{CL}}^J + \sum_{J\geqslant 1}\sigma_{\mathrm{T}}^J\Big), \tag{2.17}$$

and for the CC process is given by

$$\Big[\frac{\mathrm{d}^2\sigma_{\mathrm{i}\to\mathrm{f}}}{\mathrm{d}\Omega\mathrm{d}\mathrm{E}_{\mathrm{exc}}}\Big]_{\nu_{\mathrm{e}}/\bar{\nu}_{\mathrm{e}}} = \frac{G^2|\mathbf{k}'|E_{\mathbf{k}'}}{\pi(2J_i+1)}F(\pm Z_f, E_{\mathbf{k}'}) \times \Big(\sum_{J\geqslant 0}\sigma_{\mathrm{CL}}^J + \sum_{J\geqslant 1}\sigma_{\mathrm{T}}^J\Big), \tag{2.18}$$

where $\mathbf{k}'$ and $E_{\mathbf{k}'}$ are the three-momentum and the energy of the outgoing lepton, σ_{CL}^J is the Coulomb-longitudinal component, and σ_{T}^J is the transverse component defined as

$$\begin{aligned}\sigma_{\mathrm{CL}}^J =& (1 + a\cos\theta)|(J_f\|\mathcal{M}_J(q)\|J_i)|^2 + (1 + a\cos\theta - 2b\sin^2\theta)|(J_f\|\mathcal{L}_J(q)\|J_i)|^2 \\ &+ \frac{E_{\mathbf{k}} - E_{\mathbf{k}'}}{q}(1 + a\cos\theta + c) \times 2\mathrm{Re}[(J_f\|\mathcal{L}_J(q)\|J_i)(J_f\|\mathcal{M}_J(q)\|J_i)^*],\end{aligned} \tag{2.19}$$

and

$$\begin{aligned}\sigma_{\mathrm{T}}^J =& (1 - a\cos\theta + b\sin^2\theta) \times \big[|(J_f\|\mathcal{T}_J^{\mathrm{mag}}(q)\|J_i)|^2 + |(J_f\|\mathcal{T}_J^{\mathrm{el}}(q)\|J_i)|^2\big] \\ &\mp \frac{(E_{\mathbf{k}} + E_{\mathbf{k}'})}{q}\big(1 - a\cos\theta - c) \times 2\mathrm{Re}[(J_f\|\mathcal{T}_J^{\mathrm{mag}}(q)\|J_i)(J_f\|\mathcal{T}_J^{\mathrm{el}}(q)\|J_i)^*\big].\end{aligned} \tag{2.20}$$

Here the minus sign refers to neutrino and the plus sign to antineutrino, θ is the lepton scattering angle and $E_{\mathbf{k}}$ is the energy of the incoming (anti)neutrino. The constants in the above expressions are

$$a = \sqrt{1 - \frac{m_f^2}{E_{\mathbf{k}'}^2}}, \tag{2.21}$$

$$b = \frac{a^2 E_{\mathbf{k}} E_{\mathbf{k}'}}{q^2}, \tag{2.22}$$

$$c = \frac{m_f^2}{q E_{\mathbf{k}'}}, \tag{2.23}$$

where m_f denotes the rest mass of the outgoing lepton ($m_f = 0$ for NC process) and q is the magnitude of the three-momentum transfer

$$q = |\mathbf{q}| = \sqrt{(E_{\mathbf{k}} - aE_{\mathbf{k}'})^2 + 2aE_{\mathbf{k}}E_{\mathbf{k}'}(1 - \cos\theta)}. \tag{2.24}$$

The function $F(\pm Z_f, E_{\mathbf{k}'})$ in eq. (2.18) is known as Fermi function that takes into account the distortion of the outgoing lepton wave function due to the interaction with the final nucleus. The treatment of the final-state Coulomb effects is discussed in [34].

The definitions of the operators $\mathcal{T}_{JM} = \mathcal{M}_{JM}, \mathcal{L}_{JM}, \mathcal{T}^{\rm el}_{JM}, \mathcal{T}^{\rm mag}_{JM}$ are given in [32]. These operators depend on the nucleon form factors $F^{\rm V}_{1,2}(Q^2)$ (Vector), $F^{\rm A}(Q^2)$ (axial-vector), and $F^{\rm P}(Q^2)$ (pseudo-scalar), which depend on the four-momentum transfer Q. These form factors take into account the finite-size effects of the nucleons. The adopted form factors are presented in [33] for the NC and in [34] for the CC processes. We have assumed in the calculations a dipole form of $F_{\rm A}$ with the quenched static value $F_{\rm A}(0) = -1.00$ (at the limit of zero four-momentum transfer) and the axial-vector mass $M_{\rm A} = 1016$ MeV .

3. Results and Discussion

The performed calculations are reviewed in this chapter. The nuclear-structure computations are discussed first, and after that, the main results for the neutrino- and antineutrino-nucleus cross sections are presented and discussed. The cross sections for the neutral-current (anti)neutrino-nucleus scattering off the stable cadmium isotopes is considered in sec. 3.2. The charged-current reaction for the scattering off the stable cadmium and lead isotopes are reviewed in sec. 3.3.

3.1 Nuclear structure of the target nuclei

3.1.1 Even-mass cadmium isotopes

The QRPA was adopted to compute the required wave functions of the even-even cadmium isotopes. For this propose, the single-particle energies were obtained first from the coulomb-corrected Woods-Saxon potential with the Bohr-Mottelson parametrization [42]. The valance space consists of the orbitals 1s, 0d, 1p, 0f, 2s, 1d, 0g, 0h, 1f and 2p for both protons and neutrons. The Bonn one-boson-exchange potential [38] was used for the description of the residual two-body interaction. Then, the BCS calculations were performed to define the quasiparticles. The monopole matrix elements were scaled by adjusting the proton pairing and neutron pairing strengths so that the experimental pairing gaps, computed by the use of the three-point formula [30], were approximately reproduced. Subsequently, the QRPA method was used to compute the excited states of the even-even stable cadmium isotopes. The two-body matrix elements for the particle-particle and particle-hole parts were scaled by two parameters, $g_{\rm pp}$ and $g_{\rm ph}$. The adjustments of these parameters were done separately for each multipole J^π in such a way that the low-lying experimental excitation energy spectra were approximately reproduced (see [43, 44]).

The excitation spectra and the nuclear wave functions of the adjacent odd-odd isobars of the stable even-even cadmium nuclei were obtained by the

use of the pnQRPA method. The adjustments of the particle-hole parameters were made here via the multipole 1^+ by fixing the position of the Gamow-Teller giant resonance to the measured position [45] for ^{116}In and to the phenomenologically estimated positions [30] for the other indium nuclei. The particle-particle parameters were fixed by reproducing as well as possible the $\log ft$ values [46] of the electron-capture-decay transitions for ^{116,114,112}Cd and of the beta-minus decay transitions for the other stable cadmium isotopes. The adopted parameters are presented in [43, 47].

Another theoretical approach was adopted in [48] for the description of the nuclear wave functions that are required for the neutrino scattering off ^{116}Cd in the charged-current channel. In this approach, the pnQRPA was used with a self-consistent mean field within a valence space consisting of 15 major harmonic-oscillator shells. The two-body interaction in these computations is based on ten different globally parametrized Skyrme interactions. The considered Skyrme interactions are SkX, SkM*, SkP, UDF0, UDF1, SIII, SV, SLy4, SLy5 and SLy4d; we refer to [49] and [50] for the definitions of the Skyrme parametrizations. The code HOSPHE [39] was used to perform these calculations. The adjustments of the pairing strength G_1 were made in such a way that the energy of either the lowest proton- or neutron-quasiparticle state is equal to the empirical gap. Both empirical pairing gaps could not be reproduced simultaneously by a single value of G_1. This resulted in the adoption of a range of values for the strength G_1 for each considered Skyrme interaction, where either the proton or neutron gap was reproduced as limiting cases. The strength G_0 was chosen to be $G_0 = G_1$, which has been found to be a reasonable choice.

3.1.2 Odd-mass cadmium isotopes

The nuclear wave functions of the two odd-mass stable cadmium isotopes, i.e. ^{111}Cd and ^{113}Cd, and their neighboring odd-mass isobars were computed by the MQPM. The reference even-even nuclei were chosen as follows:

$$^{110,112}\mathrm{Cd} + \mathrm{n} \rightarrow {}^{111,113}\mathrm{Cd}, \tag{3.1}$$

$$^{110,112}\mathrm{Cd} + \mathrm{p} \rightarrow {}^{111,113}\mathrm{In}, \tag{3.2}$$

$$^{112,114}\mathrm{Cd} + \mathrm{p}^{-1} \rightarrow {}^{111,113}\mathrm{Ag}. \tag{3.3}$$

where p represents a proton-particle and p^{-1} represents a proton-hole coupled to the ground and excited states of the reference nucleus. Similarly, n denotes a neutron-particle.

In these calculations all QRPA phonons of the reference nuclei with angular momenta $J^\pi_\omega \leqslant 6\,(\pi = +, -)$ and excitation energies $E_\omega \leqslant 20$ MeV

are included. The only omitted QRPA phonons are the first (0_1^+) and second 0^+ (0_2^+) which were found to be spurious in [43, 44, 51]. The first 1^- is also omitted in order to correct for the center-of-mass spuriosity of the QRPA [52]. In [44] we found that a significant contribution from the third 0^+ state (0_3^+) appers to the configurations of some key $1/2^+$ states in ^{113}Cd after removing 0_2^+. Therefore, we have done a second MQPM calculation by omitting 0_3^+. We found that the final cross sections are practically unaffected by this procedure [44]. The adopted parameters in the MQPM calculations are the ones used in the QRPA calculations for the reference nuclei.

3.1.3 Even-mass lead isotopes

The pnQRPA was employed in [53] to construct the initial and final nuclear states that are relevant for the charged-current reactions on stable lead isotopes. The mean field and the residual interactions are treated self-consistently using the code HOSPHE [39]. We adopted a large valence space consisting of fifteen major harmonic oscillator shells, and we used three different Skyrme forces as two-body interactions, namely SkM*, SkX and SLy4 [49]. The values of the pairing strength G_1 were adopted from [54]. In the aforementioned reference there are two values related to G_1 for each interaction, so we use both values in two separate pnQRPA calculations to access the effect of pairing on the scattering observables. For the strength G_0 we used the standard recipe $G_0 = G_1$.

3.2 Neutral-Current reactions

The formalism outlined in Sec 2.2 was applied in [43, 44] to compute the cross sections for the neutral-current neutrino-nucleus scattering off the stable cadmium isotopes. The total cross sections were computed by numerical integration over the scattering angle and subsequently summing over all the discrete final states. Fig. 3.1 shows the total cross sections for the neutrino scattering off ^{111}Cd and ^{116}Cd as functions of the energy of the incoming neutrino. The total cross sections for the scattering off ^{111}Cd are a little larger in the low energy region ($E_k \leq 50$) and smaller in the high energy region ($E_k > 50$) than the cross sections for the scattering off ^{116}Cd. Similar feature could be noticed when comparing with the other even-mass cadmiums.

In the next step, the averaged cross sections are obtained by folding the computed cross sections with an appropriate neutrino spectrum. The energy spectra of supernova neutrinos in this work are described by a two-parameter

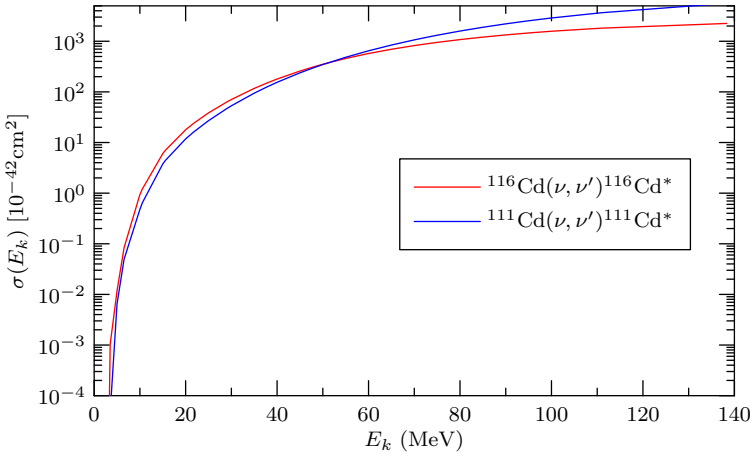

Figure 3.1: Total cross sections of the neutrino scatterings off ^{111,116}Cd as functions of the energy of the incoming neutrino.

Fermi-Dirac distribution. The averaged cross sections then takes the form

$$\langle\sigma_\nu\rangle = \frac{1}{F_2(\alpha_\nu)T_\nu^3}\int \frac{E_\nu^2\sigma(E_\nu)\mathrm{d}E_\nu}{1+\exp(E_\nu/T_\nu-\alpha_\nu)}, \tag{3.4}$$

where the parameters T_ν and α_ν represent the effective neutrino temperature and the pinching parameter, respectively. The constant $F_2(\alpha_\nu)$ normalizes the total neutrino flux to unity. In Fig. 3.2 the flux averaged neutrino cross sections for the stable cadmium isotopes are displayed. The figure shows a slight decrease in the averaged cross section in the heavy cadmiums. The odd-mass cadmiums have larger cross sections compared to the even-mass cadmiums. Similar results can be seen for the antineutrino scattering. The typical values of the (anti)neutrino parameters (T_ν, α_ν) can be derived from various supernova models [55]. For the results presented here in this thesis we adopted neutrino parameters of table 3.1.

$(\alpha_{\nu_e}, T_{\nu_e}, \langle E_{\nu_e}\rangle)$	$(\alpha_{\bar{\nu}_e}, T_{\bar{\nu}_e}, \langle E_{\bar{\nu}_e}\rangle)$	$(\alpha_{\nu_x}, T_{\nu_x}, \langle E_{\nu_x}\rangle)$	$(\alpha_{\bar{\nu}_x}, T_{\bar{\nu}_x}, \langle E_{\bar{\nu}_x}\rangle)$
(3.0, 2.88, 11.5)	(3.0, 3.41, 13.6)	(3.0, 4.08, 16.3)	(3.0, 4.08, 16.3)

Table 3.1: Values of the parameters α, T and the average neutrino energy adopted from [55]. Here x denotes the non-electron flavors, i.e. $x = \mu, \tau$.

In [43, 44] we have examined the contributions to the averaged cross sections originating from different multipole channels. Based on our results, the multipole 1^+ gives the most significant contribution. The 0^+ channel gives

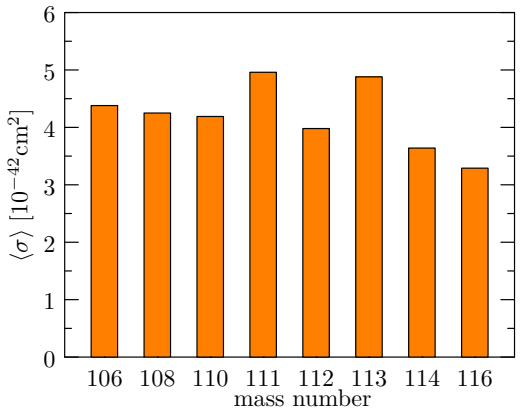

Figure 3.2: Averaged cross sections for the incoherent NC electron-neutrino scattering off the stable Cd isotopes.

also significant contribution to the averaged cross section for the odd-mass cadmium isotopes. Fig. 3.3 shows a representative plot for the neutrino scattering off ^{111}Cd and ^{116}Cd. In this figure the vector, axial vector and interference contributions to each multipole are displayed. It is seen from the figure that the 1^+ transitions are the most prominent ones and mainly of axial-vector nature while the 0^+ transitions are of vector type.

3.3 Charged-Current reactions

3.3.1 Cross sections for the stable cadmium isotopes

In the papers [43, 47, 48] we computed the cross sections for the charged-current (anti)neutrino scattering off the stable cadmium isotopes. The double differential cross section Eq. (2.18) was computed first. The total cross sections as functions of the neutrino energy were then calculated by integrating over the scattering angle and summing up the contribution coming from each final nuclear state. We found, as expected, that the total cross section increase significantly with increasing (anti)neutrino energy. The cross sections increase with increasing mass number for the neutrino scattering off the even-mass cadmiums while they decrease for the antineutrino scattering. Similar results can be observed for the scattering off the odd-mass cadmiums. The increase of the neutrino cross section with increasing mass number is explained by the increase in neutron excess which enhances the β^- branch of the GT transitions and by the lowering of the energy threshold of the neutrino scattering. The decrease in the antineutrino cross section comes from the increase in the

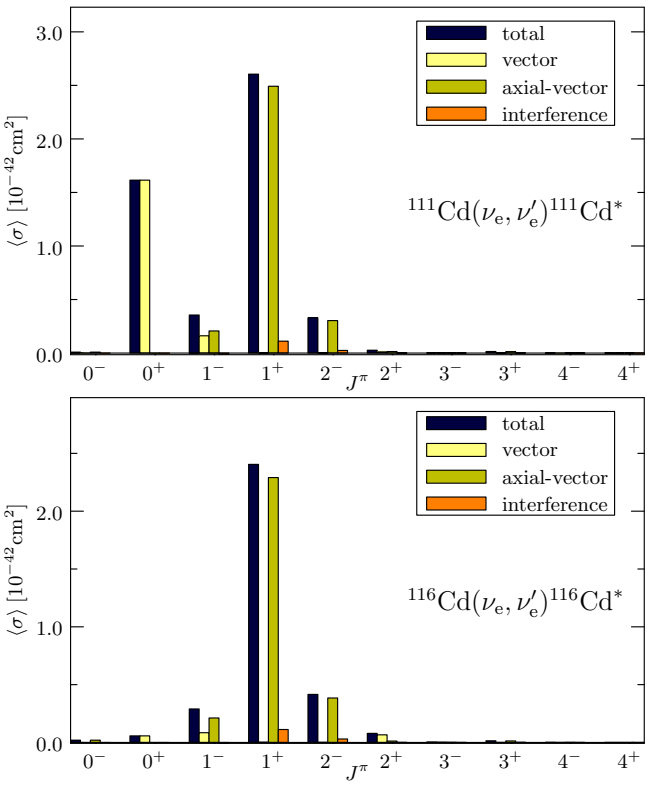

Figure 3.3: Contributions of various multipole channels to the averaged cross sections of the inchoherent neutral-current reactions on ^{111}Cd (upper panel) and ^{116}Cd (lower panel).

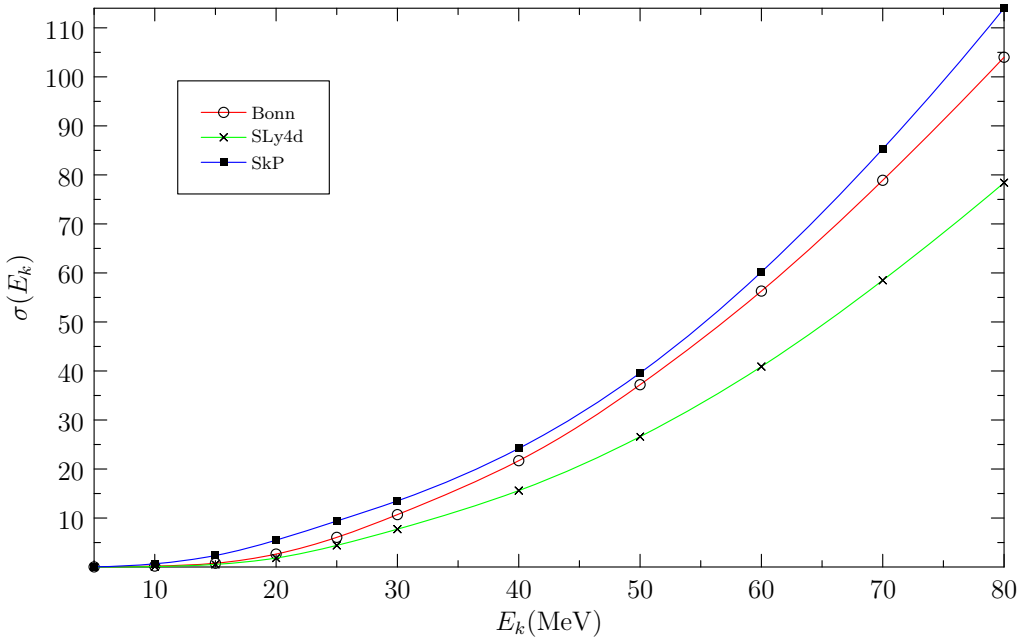

Figure 3.4: Cross sections for the charged-current neutrino scattering off ^{116}Cd in units of 10^{-42}cm^2 as functions of the energy of the impinging neutrino.

energy threshold with increasing mass number.

In [48] we compared the total cross sections for the scattering off ^{116}Cd between the calculations based on the Bonn interaction and the ones based on the Skyrme interactions. The Bonn interaction predicts cross sections for the neutrino scattering within the interval predicted by the considered Skyrme interactions. For the antineutrino scattering, all the Skyrme interactions except the SV interaction predict larger cross sections than the Bonn interaction. Fig. 3.4 shows our calculated total cross sections for the neutrino scattering off ^{116}Cd as a function of the energy of the incoming neutrino. This figure show clearly that the results of the Bonn interaction are within the interval produced by the Skyrme interactions, where the SkP force predicts the largest cross sections and the SLy4 force predicts the lowest ones.

We calculated the averaged cross section (Eq. (3.4)) by folding the computed total cross sections using the two-parameter Fermi-Dirac distribution. The resulted flux-averaged cross sections for the electron-neutrino and electron-antineutrino scattering off the Cd isotopes are displayed in Fig. 3.5. It can be concluded from this figure that the response of the odd-mass cadmiums is stronger than that of the even-mass cadmiums. The averaged cross sections depend on the mass number with opposite trend for neutrino and antineutrino scattering. This opposite trend is explained

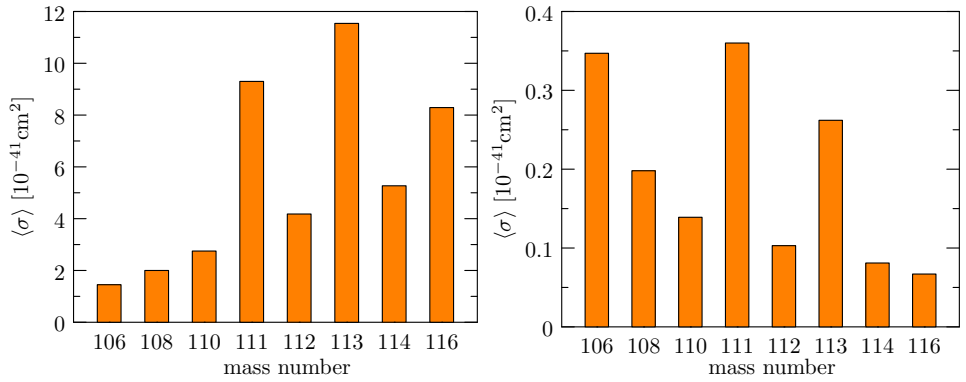

Figure 3.5: Averaged cross sections for the CC neutrino (left-panel) and antineutrino (right-panel) scattering off the stable Cd isotopes.

by the energy-threshold and the Pauli-blocking effects that are displayed schematically in Fig. 3.6. The totally different energy thresholds for the neutrino and antineutrino scatterings off the two extreme stable cadmiums are very clear in this plot. The Pauli-blocking effect is quantified in the figure by the Ikeda $3(N-Z)$ sum rule for the Gamow-Teller transitions. This sum rule gives the difference between the total (p,n) type and (n,p) type Gamow-Teller strengths, the (p,n) type strength practically exhausting the sum rule, leaving very little strength for the (n,p) type. The sum rule for the lightest cadmium is much smaller than for the heaviest one. Thus the (p,n) type of Gamow-Teller transition strength, related to the neutrino scattering, is stronger for the heavy cadmiums. On the contrary, the (n,p) type which is related to antineutrino scattering is relatively stronger for the lightest isotopes.

The averaged cross sections derived from the Skyrme interactions and the Bonn interaction for the neutrino and antineutrino scattering off ^{116}Cd are compared in table 3.2. The ranges of the cross sections for the Skyrme interactions stem from the ranges of the adopted pairing strength G_1 (see section 3.1.1). As table 3.2 shows, the SIII, SLy4 and SLy4d interactions predict rather similar averaged cross sections as the Bonn interaction for both the neutrino and antineutrino scattering. The results for neutrino scattering using the UDF forces resemble very much those of the Bonn interaction. The rest of the Skyrme interactions produce larger averaged cross sections and the SkP produces the largest one. For the antineutrino scattering, the Skyrme interactions produce larger averaged cross sections than the Bonn interaction, except for the SV interaction. The spin-isospin and isospin properties of the Bonn interaction and the considered Skyrme interactions

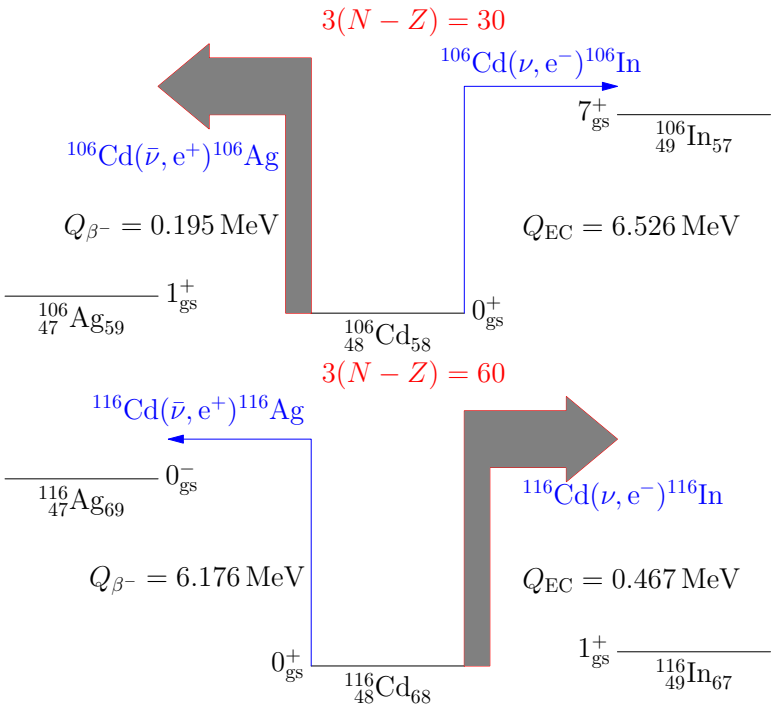

Figure 3.6: Schematic presentation of the threshold energies and Pauli blocking in the Cd chain of isotopes. The extreme cases ^{106}Cd (upper panel) and ^{116}Cd (lower panel) are displayed.

were studied and discussed in Ref [48]. Figures 3.7 and 3.8 show the calculated β^- and β^+ strength for the Gamow-Teller transitions using Bonn, UDF1 and SV interactions. The experimental position of the major satellite of the Gamow-Teller giant resonse at 14.5 MeV [45] is reproduced by the Bonn interaction and roughly by the considered Skyrme interactions except for the SV interaction as can be seen in figure 3.7. Similar results are obtained for the minor satellite at 8.9 MeV [45]. Furthermore, it was found in [48] that the total strengths for the SV interaction deviate strongly from the experimental value [45]. In figure 3.8, the strengths for the β^+ transitions is displayed. The strength is distributed between 0 and 16 MeV for the Bonn interaction while it goes to the first 1^+ for the UDF1 interaction. For the SV interaction most of the strength is coming from transitions to states around 15 MeV. In the figures one can notice that the first 1^+ state, computed by the SV interaction is far too high as compared with experiment. For the aforementioned reasons, the SV interaction was excluded when the full range, presented at the lower right corner of table 3.2, was determined. This full range of cross sections summarizes the results of all our calculations and thus gives an interval within which the true cross section most likely lies.

Incoming particle	Bonn	SkX	SkM*	SkP
ν_e	7.45	10.08-11.15	5.48-6.37	14.83-16.70
$\bar{\nu}_e$	0.067	0.096-0.101	0.100-0.106	0.135-0.141
Incoming particle	UDF0	UDF1	SIII	SV
ν_e	8.68-9.43	8.88-9.61	4.83-5.58	2.68-2.77
$\bar{\nu}_e$	0.103-0.107	0.090-0.093	0.078-0.082	0.062-0.0623
Incoming particle	SLy5	SLy4	SLy4d	Full range
ν_e	13.50-14.24	5.51-5.68	4.94-5.09	4.83-16.70
$\bar{\nu}_e$	0.115-0.119	0.077-0.079	0.075-0.076	0.067-0.141

Table 3.2: Averaged cross sections for the CC neutrino and antineutrino scattering off ^{116}Cd in units of 10^{-41}cm^2 . The lower right corner of the table, the full range, displays the interval within which all the computed results of the table fall (excluding the SV interaction, see the text for more details).

In tables 3.3 and 3.4 we present the contributions from the dominant multipole channels to the averaged cross section for neutrino scattering and antineutrino scattering off Cd isotopes, respectively. The neutrino scattering is dominated by the 1^+ multipole with axial-vector nature. The contribution of this channel is larger in the odd-mass cadmiums than in the even-mass

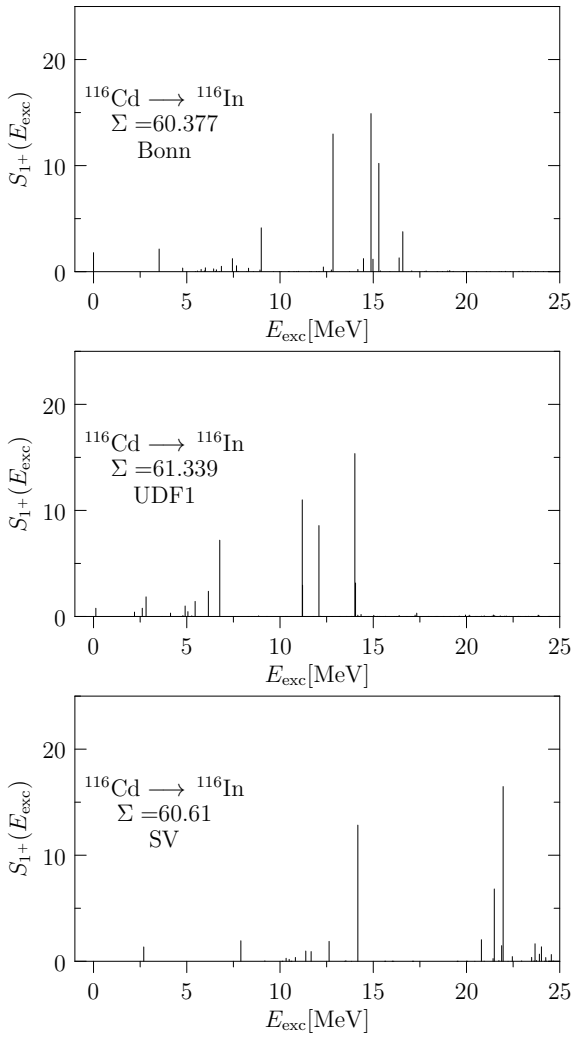

Figure 3.7: Computed β^- strength for GT transitions by Bonn, UDF1 and SV interactions.

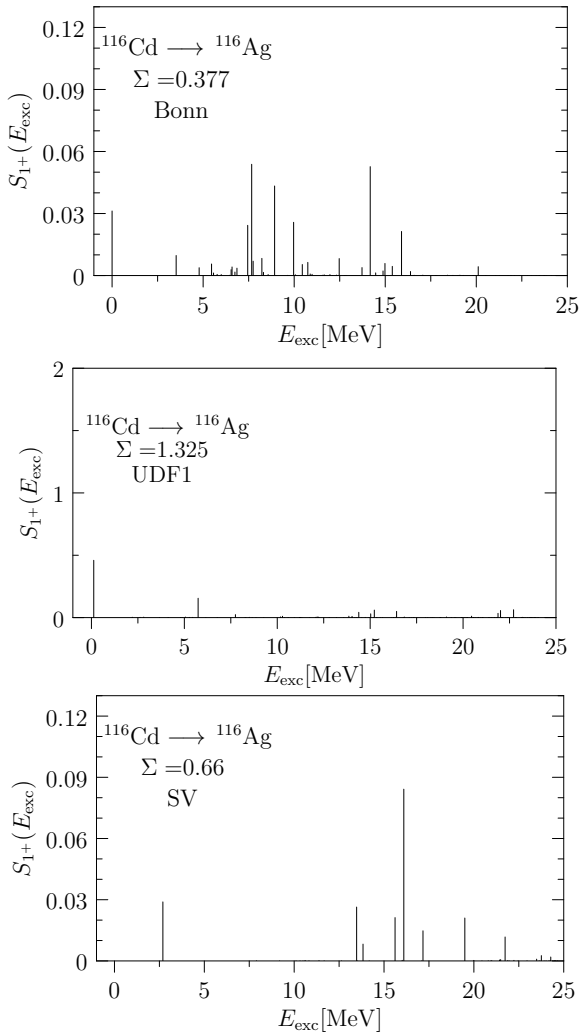

Figure 3.8: Computed β^+ strength for GT transitions by Bonn, UDF1 and SV interactions..

cadmiums. This can be explained by the different Gamow-Teller strengths in the energy region $6-10$MeV between the odd-mass and even-mass cadmiums, as discussed in [47]. The vector-type 0^+ multipole has also a significant contribution to the neutrino scattering. The 0^+ contribution is large for the odd-mass cadmiums and it enhances the cross sections for these nuclei. Further calculations are needed to extract the mechanism which causes this enhancement. It is appropriate to mention that the energies of the IAS in the indium isotopes were shifted manually to their empirical positions which were estimated in [56]. This shifting was applied before to ^{116}Cd in the calculation using the Bonn interaction in [48] and it reduces the unrealistically large 0^+ contribution found in [43]. For the antineutrino reactions the 1^- and 2^- transitions are very important. Also the 1^+ transitions contribute notably for the antineutrino scattering off the odd-mass systems and the light even-mass systems.

In figure 3.9 we show a representative case of the contributions coming from the leading multipole channels to the averaged cross sections for the CC neutrino and antineutrion scattering off ^{116}Cd using the UDF1 Skyrme force. Similar pattern can also be noticed for the other studied Skyrme interactions [48]. The only exception is for the antineutrino scattering with the SV interaction where the contribution coming from the 1^+ is very low (see [48]). It is seen in figure 3.9 that the neutrino scattering is dominated by Gamow-Teller-like transitions to 1^+ final states. The contribution of the transitions to 0^+ final state is low in this self-consistent calculation. For the antineutrino scattering the contributions come mainly from the 1^- channel. The 0^-, 1^+, and 2^- multipoles contribute also significantly. Comparing with the results of the Bonn calculation (table 3.4) we can notice that the 0^- and 1^+ contributions are larger for the Skyrme calculations. The large contribution of the 1^+ multipole stems from the large strength to the ground state of ^{116}Ag obtained in the Skyrme calculations [48].

3.3.2 Effects of the flavor transformations

In supernova-neutrino detection, only the electron (anti)neutrino can be detected in the charged-current reactions due to the large muon and tau rest masses. However, the flavor transformations in a dense supernova matter have significant effects on the energy profiles of the (anti)neutrinos in a supernova [57] . It is usually assumed that the energy spectra of muon and tau neutrinos are the same, and the three-neutrino mixing problem can be reduced to a two-neutrino problem, i.e. $\nu_x \leftrightarrow \nu_e$ where ν_x is a liner combination of ν_μ and ν_τ [58, 59]. The energy profile of the electron neutrino after the flavor conversions can be written in the form

Nucleus	0^+(V)	1^-(AV)	1^+(AV)	2^-(AV)
^{106}Cd	2.39	0.171	9.77	0.608
^{108}Cd	2.91	0.236	13.80	0.914
^{110}Cd	4.17	0.344	18.74	1.34
^{111}Cd	15.90	0.948	66.23	2.46
^{112}Cd	7.08	0.488	28.18	1.87
^{113}Cd	21.14	1.11	80.25	3.16
^{114}Cd	7.91	0.651	36.25	2.48
^{116}Cd	8.91	0.86	35.62	3.28

Table 3.3: Contributions of the prominent multipole channels to the averaged cross sections for the CC neutrino scattering in units of 10^{-42}cm^2. The label V refers to vector and AV refers to axial vector.

Nucleus	0^-(AV)	1^-(V)	1^-(AV)	1^+(AV)	2^-(AV)
^{106}Cd	0.067	0.526	0.628	2.03	0.415
^{108}Cd	0.051	0.402	0.487	0.809	0.311
^{110}Cd	0.045	0.340	0.409	0.369	0.257
^{111}Cd	0.050	0.503	0.820	2.21	0.504
^{112}Cd	0.039	0.287	0.342	0.138	0.213
^{113}Cd	0.036	0.405	0.679	1.15	0.426
^{114}Cd	0.033	0.240	0.283	0.057	0.174
^{116}Cd	0.028	0.196	0.232	0.039	0.139

Table 3.4: Same as table 3.3 for antineutrino scattering.

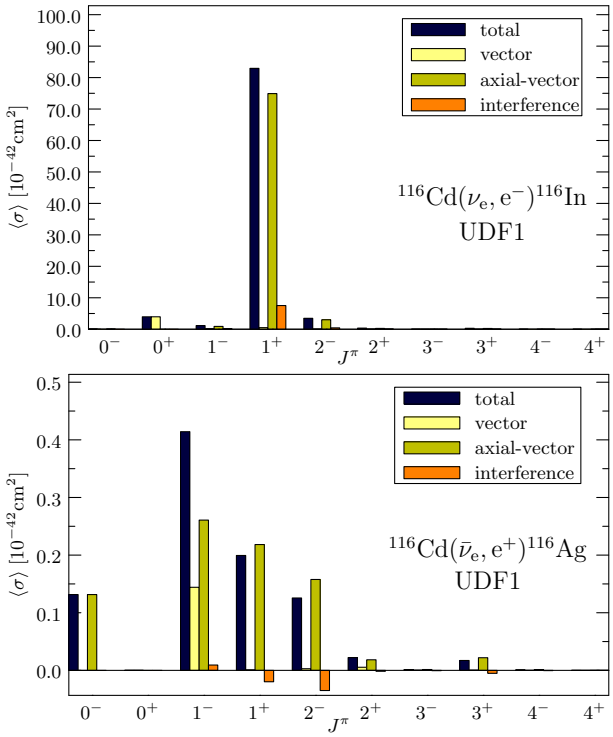

Figure 3.9: Contributions from the dominant mutipole channels to the averaged cross section for the CC neutrino scattering (upper panel) and antineutrino scattering (lower panel) off ^{116}Cd for the calculation based on the UDF1 two-body interaction.

$$F_{\nu_e}(E_{\mathbf{k}}) = \mathrm{p}(\mathrm{E}_{\mathbf{k}})\mathrm{F}^0_{\nu_e}(\mathrm{E}_{\mathbf{k}}) + (1 - \mathrm{p}(\mathrm{E}_{\mathbf{k}}))\mathrm{F}^0_{\nu_x}(\mathrm{E}_{\mathbf{k}}), \tag{3.5}$$

where $\mathrm{p}(\mathrm{E}_{\mathbf{k}})$ represents the survival probability of the electron neutrinos and $F^0_{\nu_e}(E_{\mathbf{k}})$ ($F^0_{\nu_x}(E_{\mathbf{k}})$) is the initial energy profile of the electron neutrinos (non-electron neutrinos). In a similar manner, the energy profile of the electron antineutrino can written as

$$F_{\bar{\nu}_e}(E_{\mathbf{k}}) = \bar{\mathrm{p}}(E_{\mathbf{k}})F^0_{\bar{\nu}_e}(E_{\mathbf{k}}) + (1 - \bar{\mathrm{p}}(E_{\mathbf{k}}))F^0_{\bar{\nu}_x}(E_{\mathbf{k}}). \tag{3.6}$$

Guided by [60, 61] we use for the survival probability in the case of normal mass hierarchy the prescriptions

$$\mathrm{p}(\mathrm{E}_{\mathbf{k}}) = 0, \tag{3.7}$$

and

$$\bar{\mathrm{p}}(E_{\mathbf{k}}) = \begin{cases} \cos\theta_{12} & ;\mathrm{E}_{\mathbf{k}} < \bar{\mathrm{E}}_{\mathrm{s}}, \\ 0 & ;\mathrm{E}_{\mathbf{k}} > \bar{\mathrm{E}}_{\mathrm{s}}, \end{cases} \tag{3.8}$$

where $\bar{E}_s = 18.0$ MeV [61]. Similarly, for the inverted mass hierarchy we adopt the survival probabilities

$$\mathrm{p}(\mathrm{E}_{\mathbf{k}}) = \begin{cases} \sin^2\theta_{12} & ;\mathrm{E}_{\mathbf{k}} < \mathrm{E}_{\mathrm{s}}, \\ 0 & ;\mathrm{E}_{\mathbf{k}} > \mathrm{E}_{\mathrm{s}}, \end{cases} \tag{3.9}$$

and

$$\bar{\mathrm{p}}(E_{\mathbf{k}}) = \cos^2\theta_{12}, \tag{3.10}$$

with the value $E_s = 7$ MeV [58]. In the present computations we employ for $\sin^2\theta_{12}$ the values of [62], i.e. 0.306 (0.312) for the normal (inverted) hierarchy.

The effects of oscillations on the averaged cross sections can be seen in Fig. 3.10 . Our results for neutrino scattering are almost independent of the neutrino mass hierarchy and therefore we present in the figure the result only for the normal hierarchy. In contrast to the neutrino scattering, the antineutrino scattering in the normal mass hierarchy has larger cross sections than in the inverted mass hierarchy. An implication of this is the possibility to distinguish between the two mass-hierarchies in very large neutrino telescopes with good background rejection. Moreover, Fig. 3.10, when compared with Fig. 3.5, shows that the averaged cross sections increase significantly when the flavor transformations are included.

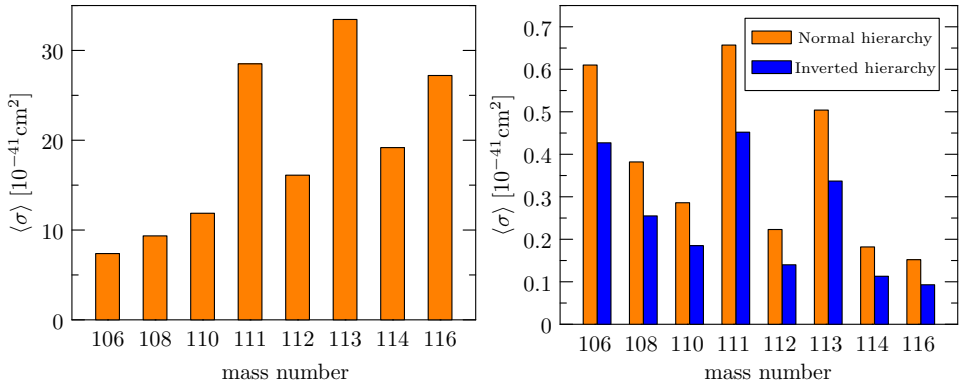

Figure 3.10: Averaged cross sections for the CC neutrino (left-panel) and antineutrino (right-panel) scattering off Cd isotopes including the effect of oscillations. For the neutrino scattering only the results for the normal hierarchy are plotted.

3.3.3 Cross sections for the stable even-even lead isotopes

The charged-current cross sections of the neutrino and antineutrino scattering off the stable even-even lead isotopes was computed in [53]. In this study we follow the scheme of [48] by performing self-consistent calculations that are based on the Skyrme forces SkM*, SLy4 and SkX.

In [48] the properties of various isovector excitation of ^{116}Cd were considered first. Here we do the same for ^{208}Pb. Table 3.5 presents the computed positions of the IAS, the energy centroids of the GTGR and the strengths related to the GTGR in ^{208}Bi. The experimental values [63] are also shown in the table. The two values of the computed results come from the two adopted values for the pairing strength (see sec. 3.1.3). The IAS position computed by the SLy4 is the closest one to the experimental position. The SkM* predicts a lower position and the SkX predicts a higher one. The computed centroids of the GTGR are shifted up for the SkM* and SLy4 while it is shifted down for the SkX as compared with the experimental centroid. The computed GTGR strengths are inside the measured interval for all the interactions. The computed strengths have been multiplied by a factor of 0.56 to allow comparison with the experimental data [63] where only 56% of the total strength given by the Ikeda sum rule was observed. The cumulative β^- strength for the GT transitions is shown in figure 3.11. Both SLy4 and SkM* give better results than the SkX as compared with the experimental data. One can conclude that concerning the isovector properties the SkX interaction performs inferior to the other two interactions. The performance

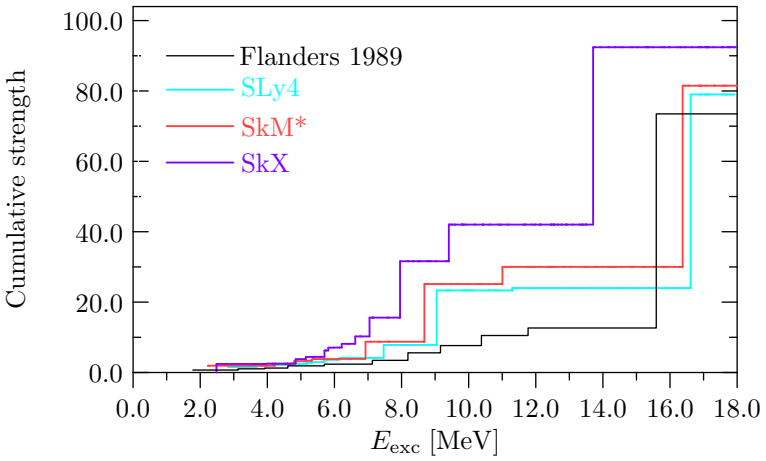

Figure 3.11: Cumulative β^- strengths for the GT transitions. Fanders 1989 refers to Ref.[63].

of the SkM* and SLy4 interactions is roughly at the same level.

	SkM*	SkX	SLy4	Expt [63]
Positions of the IAS	15.49,15.43	18.62,18.66	16.79,16.73	17.47
Centroids of the GTGR	16.43,16.37	13.74,13.71	16.90,16.84	15.23
GTGR β^- strength	51.48	50.39	55.0	60.84 $\pm$13.67

Table 3.5: Computed and experimental positions of the IAS, centroids and the strengths of the GTGR in ^{208}Bi. The energies are in MeV.

The computed cross sections for the scattering off ^{208}Pb are compared with two earlier calculations [64, 65] and extended to take into account the effects of neutrino oscillations. The comparison of the total cross sections is visible in figure 3.12 . Our obtained results are in good agreement with [65] for small neutrino energies ($E_\nu < 30\,\text{MeV}$) while both [64] and [65] predict larger total cross sections for high neutrino energies ($E_\nu > 30\,\text{MeV}$). For the antineutrino scattering, it was possible to compare our results with [64] and we found in [53] that our total cross sections are much larger than in the aforementioned reference. The reason for such a deviation is hard to be identified. In terms of the used interactions, ref. [65] used different type of interaction and also different approach for the final-state Coulomb effects. However, ref. [64] used similar approaches using the SIII Skyrme interaction. It is worth mentioning that the results of [64] deviate also from the similar calculations of [66, 67] where, likewise, the SIII force was used.

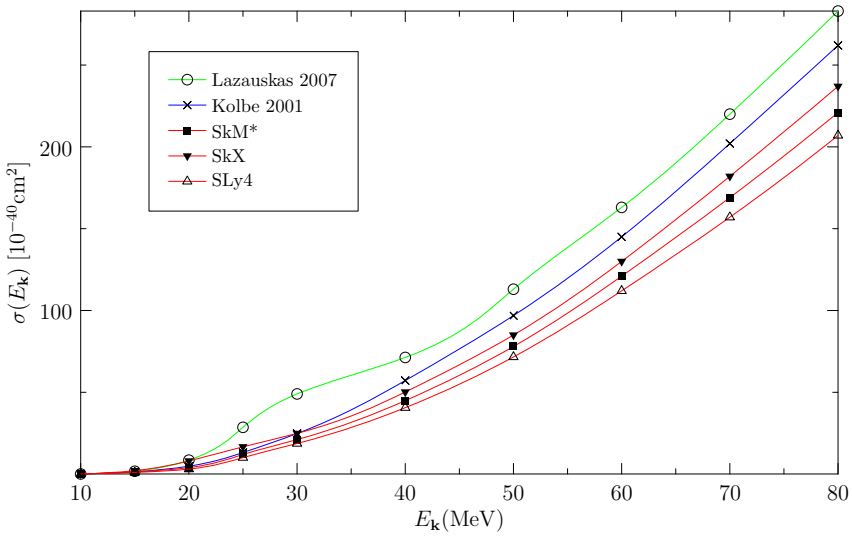

Figure 3.12: Comparsion of our total cross section for neutrino scattering off ^{208}Pb and those of Lazauskas 2007: Ref.[64] and Kolbe 2001: Ref. [65].

The flux-averaged cross sections are computed using eq. (3.4). For ^{208}Pb, we achieved a very good agreement with the results of Ref. [65] for neutrino scattering. In the case of antineutrino scattering our results are slightly larger. Table 3.6 shows the computed averaged cross sections for the charged-current neutrino and antineutrino scatterings off the stable lead nuclei using the parameters of table 3.1. The ranges presented in table 3.6 summarize all our computations, i.e. using the three Skyrme forces and the two adopted values of the pairing strength. The table shows that the averaged cross sections for neutrino scattering do not vary notably from one lead nucleus to the other as opposed to antineutrino scattering. The nuclear responses increase when the neutrino oscillations are included. The cross sections are independent of the mass-hierarchy for the neutrino scattering, whereas the cross sections for the antineutrino are larger in the normal mass hierarchy than in the inverted mass hierarchy. Fig. 3.13 visualizes the effects of the oscillations for the neutrino and antineutrino scattering off ^{208}Pb. The difference between the effects of the two hierarchies are clearly visible in the right panel of the figure.

In order to examine which final states contribute to the averaged cross section the most, we plot in figure 3.14 the cumulative cross sections as functions of the excitation energy of the final state. As seen from the upper panel of this figure, the major contribution for the neutrino scattering comes from the Gamow-Teller gaint resonane, GTGR. A small step at the location of the IAS can also be noticed. The notable contribution within the range $1-14$

Nucleus	ν_e	ν_{ex}^{NH}	ν_{ex}^{IH}
^{204}Pb	9.74-18.63	38.00-63.15	38.09-62.40
^{206}Pb	9.94-19.70	38.59-66.24	38.69-65.61
^{208}Pb	9.89-18.75	38.67-64.65	38.82-63.79
Nucleus	$\bar{\nu}_e$	$\bar{\nu}_{ex}^{NH}$	$\bar{\nu}_{ex}^{IH}$
^{204}Pb	0.188-0.222	0.380-0.427	0.248-0.285
^{206}Pb	0.111-0.146	0.245-0.301	0.153-0.194
^{208}Pb	0.084-0.096	0.199-0.220	0.120-0.135

Table 3.6: Averaged cross sections for the charged-current neutrino and antineutrino scattering off the stable lead nuclei in units of 10^{-41}cm^2. Here ν_e and $\bar{\nu}_e$ denote the nonoscillating case, while ν_{ex}^{NH} (normal hierarchy) and ν_{ex}^{IH} (inverted hierarchy) correspond to oscillating cases.

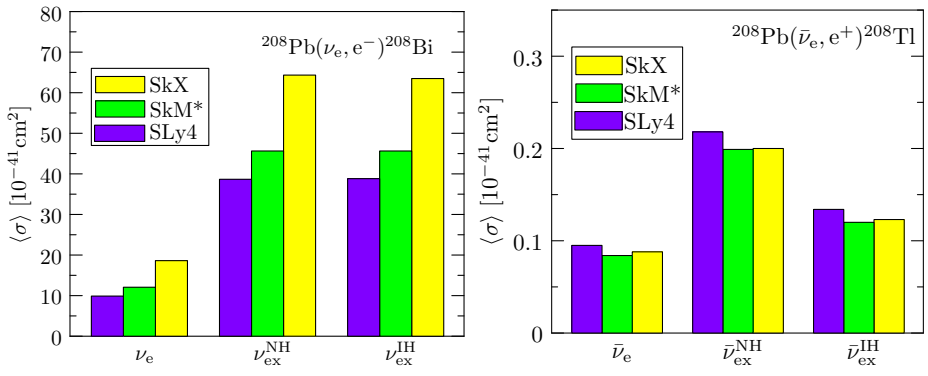

Figure 3.13: Averaged cross sections for the CC neutrino (left panel) and antineutrino (right panel) scattering off ^{208}Pb.

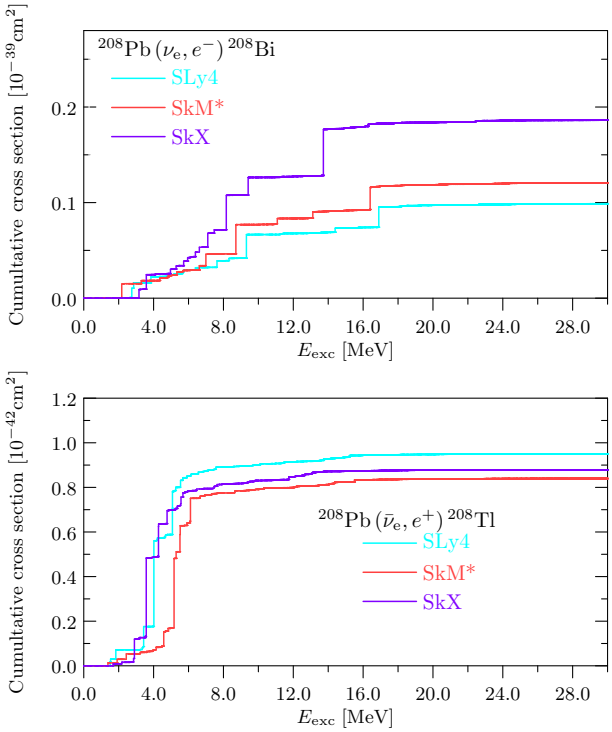

Figure 3.14: Cumulative sums of the averaged cross sections for the neutrino (upper panel) and antineutrino (lower panel) scattering off ^{208}Pb.

MeV comes mostly from Gamow-Teller transitions to 1^+ states. Our computed positions of the GTGR and IAS are presented in [53] and compared with the experimental values of [63]. The cumulative sums for the antineutrino, lower panel of figure 3.14, saturate very early at energies around $5 - 9$ MeV. The results for ^{204}Pb and ^{206}Pb are very similar to the ones of ^{208}Pb for neutrino scattering, whereas for the antineutrino scattering the results vary notably from nucleus to nucleus. For example, the largest cross section is obtained by the SLy4 interaction for ^{208}Pb and by the SkX interaction for ^{204,206}Pb. Also, the relevant contributions to antineutrino scattering off ^{208}Pb come from much lower energies than in the case of ^{204,206}Pb.

Finally, we studied the contributions coming from the leading multipole channels to the averaged cross sections. We found that the neutrino scattering is dominated by the 1^+ multipole of axial-vector type. For the antineutrino reactions the contributions stem mainly from the 1^- multipole of axial-vector nature. Also the 0^-, 2^- and 1^+ channels contribute notably to the antineutrino scattering.

4. Conclusions

Computations of the neutrino- and antineutrino-nucleus scattering cross sections are performed and reported in this thesis. The neutral-current and charged-current (anti)neutrino-nucleus cross sections are calculated for the stable cadmium isotopes ($A = 106, 108, 110, 111, 112, 113, 114, 116$). The charged-current cross sections for (anti)neutrino scattering off the stable lead isotopes ($A = 204, 206, 208$) are also computed. The ranges of neutrino energies treated in this work are appropriate for the case of supernova neutrinos.

Accurate nuclear models are required to describe the wave functions of the initial and final states involved in the scattering processes. The quasiparticle random-phase approximation (QRPA) is used in our work to treat the even-mass cadmium and lead nuclei and the microscopic quasiparticle-phonon model (MQPM) to compute the properties of the odd-mass cadmium nuclei. The QRPA calculations for the cadmium isotopes were based on the Bonn one-boson-exchange potential and the parameters of the Hamiltonian were adjusted locally. Self-consistent calculations based on different Skyrme interactions were performed for the lead isotopes. The study of the charged-current processes in ^{116}Cd was extended to self-consistent Skyrme-based calculations allowing comparison with the earlier Bonn-based calculations. Such comparison could provide an overview on the impact of the adopted theoretical approach on the final cross section.

The differential scattering cross sections are obtained by expanding the nuclear weak current in multipoles. The final cross sections are then obtained by integrating over the scattering angle. Subsequently, the nuclear responses to supernova neutrinos were calculated by folding the obtained cross sections with a two-parameter Fermi-Dirac distribution. The impact of the neutrino flavor transformations in an exploding supernova on the flux-averaged cross sections was also studied for the charged-current reactions in order to assess the potential discrimination between the two neutrino-mass hierarchies in future large neutrino telescopes.

Our calculations show that the nuclear responses of the odd-mass cadmi-

ums to the supernova (anti)neutrinos are much stronger than those of the even-mass cadmiums. The averaged cross sections for the neutral-current reactions are almost independent of the mass number for the even-mass cadmiums and also for the odd-mass ones. Contrariwise, the averaged cross sections for the charged-current neutrino scattering off the light cadmiums are notably smaller than off the heavy cadmiums, and vice versa for the antineutrino scatterings. In the case of lead isotopes, there is no drastic dependence on the mass number for the neutrino scattering while slight decreasing trend can be noticed for the antineutrino scattering.

Furthermore, We have found that the transitions to the 1^+ states are the most important ones for the neutral-current and charged-current neutrino scattering off the stable lead and cadmium isotopes. The 0^+ channel is also important for the neutral-current neutrino scattering off the odd-mass cadmium isotopes. For the charged-current antineutrino scattering, the transitions to the 1^- and 2^- multipole states are the most important ones, except for the scattering off the light cadmiums (^{106}Cd,^{108}Cd) and odd-mass cadmiums where the 1^+ multipole is the dominate one. The 1^+ channel is also important in the Skyrme-based calculations.

According to our calculations the charged-current (anti)neutrino cross sections are significantly enhanced by the neutrino-flavor transformations. We found, for the considered supernova scenarios, that the neutrino cross sections are almost independent of the neutrino-mass hierarchy. However, the cross sections for the antineutrino scattering are quite different for the normal and inverted mass hierarchy. This could have interesting consequences for the future large-scale neutrino telescopes which can be used, in principle, to determine the nature of the neutrino mass hierarchy.

Bibliography

[1] K. Scholberg, Ann. Rev. Nucl. Part. Sci. 62 (2012) 81.

[2] C. Hargrove, I. Batkinb, M. Sundaresan, J. Dubeau, Astro. Part. Phys 5 (1996) 183.

[3] K. Zuber, Nucl. Part. Phys. Proc. 265-266 (2015) 233.

[4] Helium, Lead Observatory, http://www.snolab.ca/halo/.

[5] K. Langanke, Nucl. Phys. A 834 (2010) 608c.

[6] K. Langanke, G. Martínez-Pinedo, Rev. Mod. Phys. 75 (2003) 819.

[7] J. Gava, C. Volpe, AIP Conf. Proc. 1038 (2008) 193.

[8] C. Volpe, J. Phys. G: Nucl. Part. Phys 31 (2005) 903.

[9] J. D. Vergados, H. Ejiri, F. šimkovic, Rep. Prog. Phys. 75 (2012) 106301.

[10] F. T. Avignone III, S. R. Elliott, J. Engel, Rev. Mod. Phys. 80 (2008) 481.

[11] J. Ebert, et al., Phys. Rev. C 94 (2016) 024603.

[12] J. Suhonen, O. Civitarese, Phys. Rep. 300 (1998) 123.

[13] J. Barea, J. Kotila, F. Iachello, Phys. Rev. C 87 (2013) 014315.

[14] J. Hyvärinen, J. Suhonen, Phys. Rev. C 91 (2015) 024613.

[15] S. K. Singh, N. C. Mukhopadhyay, E. Oset, Phys. Rev. C 57 (1998) 2687.

[16] E. Kolbe, K. Langanke, E. Vogel, Nucl. Phys. A 652 (1999) 91.

[17] N. Jachowicz, S. Rombouts, K. Heyde, J. Ryckebusch, Phys. Rev. C 59 (1999) 3246.

[18] N. Jachowicz, K. Heyde, J. Ryckebusch, S. Rombouts, Phys. Rev. C 65 (2002) 025501.

[19] A. Botrugno, G. Co', Nucl. Phys. A 761 (2005) 200.

[20] N. Paar, D. Vretenar, T. Marketin, Phys. Rev. C 77 (2008) 024608.

[21] H. Dapo, N. Paar, Phys. Rev. C 86 (2012) 035804.

[22] A. R. Samana, F. Krmpotic, N. Paar, C. A. Bertulani, Phys. Rev. C 83 (2011) 024303.

[23] W. C. Haxton, Phys Rev. D 36 (1987) 2283.

[24] T. Suzuki, et al., Phys. Rev. C 79 (2009) 061603(R).

[25] A. A. Dzhioev, A. I. Vdovin, G. Martínez-Pinedo, J. Wambach, C. Stoyanov, Phys. Rev. C 94 (2016) 015805.

[26] K. G. Balasi, E. Ydrefors, T. S. Kosmas, Nucl. Phys. A 868-869 (2011) 82.

[27] E. Ydrefors, J. Suhonen, Y. M. Zhao, Phys. Rev. C 91 (2015) 014307.

[28] M. K. Cheoun, E. Ha, K. S. Kim, T. Kajino, J. Phys. G: Nucl. Part. Phys. 37 (2010) 055101.

[29] D. Vale, N. Paar, arXiv:1406.2584v1 [nucl-th].

[30] J. Suhonen, From Nucleons to Nucleus: Concepts of Microscopic Nuclear Theory, Springer, Berlin, 2007.

[31] J. Toivanen, J. Suhonen, Phys. Rev. C 57 (1998) 1237.

[32] J. D. Walecka, Theoretical Nuclear and Subnuclear Physics, Imperial College Press, London, 2004.

[33] E. Ydrefors, K. G. Balasi, J. Suhonen, T. S. Kosmas, Nuclear Responses to Supernova Neutrinos for the Stable Molybdenum Isotopes, Neutrinos: Properties, Reactions, Sources and Detection, Nova Science Publishers, 2011.

[34] E. Ydrefors, J. Suhonen, Advances in High Energy Physics 2012 (2012) 373946.

[35] J. Bardeen, L. N. Cooper, J. R. Schriffer, Phys. Rev. 108 (1957) 1175.

[36] A. Bohr, B. R. Mottelson, D. Pines, Phys. Rev. 110 (1958) 936.

[37] J. Suhonen, Nucl. Phys. A 563 (1993) 205.

[38] K. Holinde, Phys. Rep. 68 (1981) 121.

[39] B. G. Carlsson, J. Dobaczewski, J. Toivanen, P. Vesely, Comp. Phys. Commun. 181 (2010) 1641.

[40] P. Veselý, J. Toivanen, B. Carlsson, J. Dobaczewski, N. Michel, A. Pastore, Phys. Rev. C 86 (2012) 024303.

[41] B. G. Carlsson, J. Toivanen, Phys. Rev. C 89 (2014) 054324.

[42] A. Bohr, B. R. Mottelson, Nuclear Structure, Benjamin, New York, 1969.

[43] W. Almosly, E. Ydrefors, J. Suhonen, J. Phys. G: Nucl. Part. Phys. 40 (2013) 095201.

[44] W. Almosly, E. Ydrefors, J. Suhonen, J. Phys. G: Nucl. Part. Phys. 42 (2015) 025106.

[45] H. Akimune, et al., Phys. lett.B 394 (1997) 23.

[46] National Nuclear Data Center, http://www.nndc.bnl.gov.

[47] W. Almosly, E. Ydrefors, J. Suhonen, J. Phys. G: Nucl. Part. Phys. 42 (2015) 095106.

[48] W. Almosly, B. G. Carlsson, J. Dobaczewski, J. Suhonen, J. Toivanen, P. Vesely, E. Ydrefors, Phys. Rev. C 89 (2014) 024308.

[49] M. Dutra, et al., Phys. Rev. C 85 (2012) 035201.

[50] M. Kortelainen, et al., Phys. Rev. C 85 (2012) 024304.

[51] M. Baranger, Phys. Rev. 120 (1960) 957.

[52] P. Ring, P. Schuck, The Nuclear Many-Body Problem, Springer, Berlin, 1980.

[53] W. Almosly, B. G. Carlsson, J. Suhonen, J. Toivanen, E. Ydrefors, Phys. Rev. C 94 (2016) 044614.

[54] B. G. Carlsson, J. Toivanen, A. Pastore, Phys. Rev. C 86 (2012) 014307.

[55] M. T. Keil, G. G. Raffelt, Astrophys. J. 590 (2003) 971.

[56] Y. Z. Qian, W. C. Haxton, K. Langanke, P. Vogel, Phys. Rev. C 55 (1997) 1532--1544.

[57] B. Dasgupta, A. Dighe, G. G. Raffelt, A. Yu Smirnov, Phys. Rev. Lett. 103 (2009) 051105.

[58] J. Gava, C. Volpe, Phys. Rev. D 78 (2008) 083007.

[59] A. B. Balantekin, G. M. Fuller, J. Phys. G: Nucl. Part. Phys. 29 (2003) 2513.

[60] G. G. Raffelt, Prog. Part. Nucl. Phys 64 (2010) 393.

[61] G. Martínez-Pinedo, B. Ziebarth, T. Fischer, k. Langanke, Eur. Phys. J. A 47 (2011) 98.

[62] K. Nakumura, et al., J. Phys. G: Nucl. Part. Phys. 37 (2010) 075021.

[63] B. S. Flanders, R. Madey, B. D. Anderson, A. R. Baldwin, J. W. Watson, C. C. Foster, H. V. Klapdor, K. Grotz, Phys. Rev. C 40 (1989) 1985.

[64] R. Lazauskas, C. Volpe, Nucl. Phys. A 792 (2007) 219.

[65] E. Kolbe, K. Langanke, Phys. Rev. C 63 (2001) 025802.

[66] C. Volpe, N. Auerbach, G. Colò, N. Van Giai, Phys. Rev. C 65 (2002) 044603.

[67] J. Engel, G. C. McLaughlin, C. Volpe, Phys. Rev. D 67 (2003) 013005.